Fracture behavior of flax fibers reinforced earth concrete

Nathalie Kouta, Jacqueline Saliba, Nadia Saiyouri

Fracture behavior of flax fibers reinforced earth concrete

KOUTA Nathalie, SALIBA Jacqueline, SAIYOURI Nadia

Université de Bordeaux, UMR 5295, Institut de Mécanique et d'Ingénierie (I2M), CNRS, Esplanade des Arts et Métiers, 33405 Talence, France

Abstract. The mechanical behavior of earth concrete for sustainable construction has been studied in this paper. The effect of flax fibers on the fracture behavior has been monitored using digital image correlation (DIC) and acoustic emission (AE) techniques to better understand the fracture process and damage mechanism. Three-point bending tests have been conducted on prismatic specimens with different percentages (0%, 0.3% and 0.6%) and lengths (12 mm, 24 mm, 50 mm) of flax fibers. The AE activity and fracture energy increased with the percentage and length of fibers. Moreover, the AE signal parameters varied with the loading rate and different damage mechanisms have been distinguished. Crack opening resistance also increased due to the bridging effect of fibers along developed cracks. Those results show the benefits of adding flax fibers to enhance the ductility of earth concrete.

Keywords: Earth concrete, Flax fibers, Damage, Digital Image Correlation, Acoustic Emission technique.

1. Introduction

The continuous increase of energy consumption, greenhouse gas emissions and natural resources depletion has created many problems that need to be addressed during the upcoming years [1].The construction field is responsible for 50% of the annual global carbon-dioxide emissions [2]. Thus, the need for an alternative material that is eco-friendly and sustainable has become essential to reduce environmental impacts [3–8]. The use of earth concrete can be an alternative to standard concrete in the construction of elements not requiring high mechanical performance. Earth concrete is constituted of soil stabilized with lime and cement and can be

poured similar to classic concrete. It has a low energy consumption, especially during the production process, since it is constituted of local and natural raw material and presents good hygrothermal properties [9].

Natural fibers are widely used in earth construction. Using natural/vegetal fibers instead of artificial fibers can reduce the weight, cost and energy consumption of earth concrete [10]. Furthermore, these biodegradable and nontoxic fibers are known by their good thermal and acoustic insulation properties [10–13]. The use of natural fibers can also improve the mechanical behavior and reduce the plastic shrinkage cracking of concrete. The presence of clay in earth concrete makes it sensitive to early age shrinkage cracking, hence adding fibers to the mixture can be beneficial [14]. In addition, the brittle rupture and low mechanical performance of earth concrete subjected to tensile stress are the reasons behind the necessity of using fibers. The addition of fibers can lead to a higher tensile and flexural strength and significantly improve the ductility of concrete as the stress is transferred between the matrix and fibers during loading [15]. The fracture process in fiber reinforced concrete presents different failure mechanisms such as the fracture of the mortar, the plastic deformation induced by the interface debonding between the matrix and the fibers due to fiber pull out and fiber rupture [16,17]. The fibers lead to bridge the crack sides and increase the crack opening resistance[15,16]. However, one of the main disadvantages of using natural fibers is their degradation in alkaline environment due to the degradation of the main chemical component of these fibers, cellulose, by depolymerization known as the peeling off reaction [18,19]. Therefore, their mechanical properties and their effectiveness can be reduced [20]. The comparison between different types of natural fibers and their impact on the mechanical behavior of earth concrete is difficult to quantify due to the large variety of natural fibers that could be sorted by type, properties, shape, length, strength, cohesion and water absorption in addition to their percentage and concrete mixtures [21–23]. In this study, flax fibers have been used. Flax fibers are natural, ecological with no harmful effect on the environment even after their degradation and have an economic benefit compared to synthetic fibers. They are flexible due to the high length/diameter ratio and have good tensile strength and bond properties with concrete [7].

The AE technique is a non-destructive technique widely used recently for damage monitoring [24]. It offers a high sensitivity for damage detection and allows us to understand the fracture behavior of concrete [24–30]. It results from the creation of transient elastic waves due to the release of energy by different sources in the material as friction and micro-cracking. Elastic waves propagate from the source inside the material to the surface where they could be detected by piezoelectric sensors. The sensors record the response and convert the vibration into an electrical signal. The obtained signals are then amplified in order to be analyzed correctly. The AE parameters (amplitude, energy, average frequency…) can be correlated to the source, intensity and type of fracture [31–33]. The relationship between the average frequency (AF) and the RA value (the rise time over the maximum amplitude of the waveform) can be also used to classify the tensile and shear rupture modes [34,35]. The fracture behavior of fiber reinforced concrete using the AE technique have been evaluated in the literature [31,36–42]. The results show that the addition of fibers leads to an increase of the AE activity [31]. However, no previous investigation studied the effect of fibers on the mechanical behavior of earth concrete.

The DIC technique has been highly employed for crack monitoring due to its simplicity and high resolution [43,44]. The displacement field of the specimen surface can be deduced due to the tracking of the speckle pattern applied on the surface. Based on the displacement field and using the finite element shape functions, the strain field can be calculated [45–47]. This method has been also used in this study to investigate the cracking propagation [46,48–50].

The main objective of this paper is to study the effect of different lengths and percentages of non-treated flax fibers on the fracture behavior of earth concrete during flexural tests. These tests were monitored in parallel with the DIC and the AE techniques. The materials and experimental techniques are first presented. Then, the AE and DIC results are exposed and the effect of fibers is analyzed.

2. Experimental program

2.1. Materials

Artificial soil has been used to overcome the discrepancies of natural soil. It is composed of 30% of clayey soil (which mineralogical composition is 75% of smectite, 15% of illite, 10% of Kaolinite) and 70% of sand. The clay is sourced from Lafaure and has a liquid and plastic limit of 84.6% and 29.2% respectively. The soil has been stabilized with two types of hydraulic binders: the natural hydraulic lime NHL5 in accordance with the European standard EN 459-1 and the cement CEM 1, 52.5 N PM-CP2 according to NF EN197-1 standard. The mixture composition of lime and cement is respectively 3% and 8% of the overall quantity of clay / sand mixture. These percentages have been set according to different studies concerning the effect of the percentage of stabilizer on the properties of earth concrete [51–54].

The mixture has been realized by first mixing clay and sand to ensure a certain homogeneity. Then, lime and cement have been added to the dry mixture before the addition of water and superplasticizer (Tempo 10).

Natural flax fibers, cut at constant lengths of 12, 24 and 50 mm with diameters equal to 14.66 µm ±2.95, are used [55]. These fibers are rich in cellulose and have good tensile strength properties [7]. However, all natural fibers are hydrophilic which may affect the workability and the behavior of earth concrete [56,57]. The coefficient of absorption of fibers is (105 ± 5%). Additional information about the constituents and mixtures properties at early age can be found in [14].

2.2. Mixtures composition

Seven mixtures have been tested by varying the percentage (0; 0.3 and 0.6%) and length (12; 24 and 50 mm) of fibers. These mixtures are named following this method: [SA (%fibers) F (length)]. **Table 1** presents the composition of these mixtures. The quantity of added fibers is subtracted from the artificial soil mass to maintain a constant solid mass. The effective water to binder ratio has

been kept constant and equal to 0.45. Additional water has been added to account for the water absorbed by flax fibers.

Table 1. *Mixtures composition*

Components (kg/m^3)	Sand	Bentonite	Cement	Lime	Effective water	Total water	Super-plasticizer	Flax fibers
SA0F0	931	405	152	34.2	83.8	367	1.6	0
SA03F12/24/50	929	401	152	34.2	83.8	370	1.6	5.7
SA06F12/24/50	925	399	152	34.2	83.8	375	1.6	11.4

2.3. Three-point bending test

Flexural tests have been performed on prismatic specimens of 7 x 7 x 28 cm^3 (**Figure 1**). Specimens have been removed from molds 24 hours after casting and stored at a relative humidity of 90% and a temperature of 20°C. Flexural tests have been conducted at the age of 28 days using an electromechanical machine with a capacity of 100 kN. The three-point bending test has been controlled with a constant loading displacement rate of 0.15 mm/min.

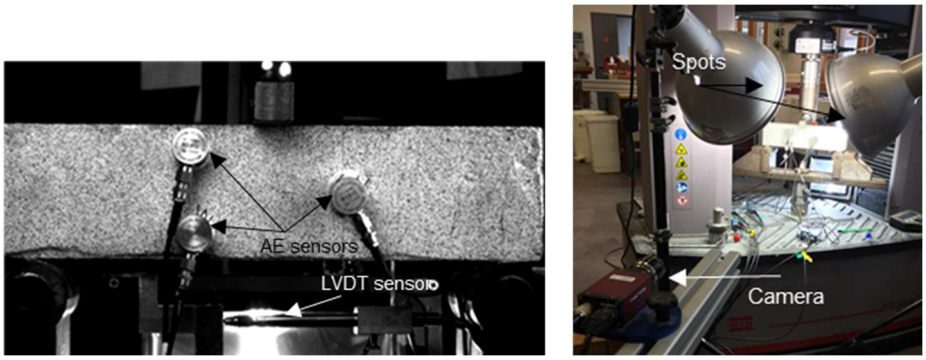

Figure 1: *Flexural test setup*

2.4. Digital image correlation technique

Flexural tests have been monitored with the DIC technique, which is a direct and simple method for fracture examination. This technique requires the surface preparation of earth concrete specimens prior to the test by using a white and black speckle (white paint at the bottom with small

125 black dots above). The displacement of the tested surface is obtained by the analysis of the random
126 speckle at different times based on the pictures taken during the test. The photos of the specimen's
127 surface have been captured using a digital camera with a resolution of 2452 × 2056 pixels. To
128 improve the photo brightness, two lamps have been used in parallel. Images have been taken at a
129 rate of one image per second during the test and stored directly. Image processing treatment has
130 been realized using the commercial Vic 2D software with a resolution of 0.05 mm per pixel.
131 However, this technique does not give enough information about the microstructure damage as
132 the obtained results remain at the surface of the specimen and cannot show damage volume
133 evolution. Thus, the AE technique has been also used.
134

135 ## 2.5.Acoustic emission technique

136 The used AE system consists of an eight channel AEWIN system with a general- purpose
137 interface bus and a system for data storage analysis. A 3D localization algorithm has been used for
138 the localization of AE events. 6 R15a piezoelectric sensors were used (**Figure 2**) with a frequency
139 range between 50 and 200 kHz and a resonance frequency of 150 kHz. The sensors were placed on
140 two opposite sides of the specimen using a thin layer of silicone grease expelled from air to ensure
141 a good coupling between the specimen and the sensors. The transducers were placed around the
142 cracking propagation area. The detected signals were amplified with a 40 dB gain differential
143 amplifier. One of the main disadvantages of this technique is the lack of reproducibility due to the
144 nature of the source signals (random cracks) and the presence of surrounding environment noise.
145 The detection threshold is set at 35 dB to avoid the background noise. The acquisition system was
146 calibrated before each test using a pencil lead break procedure. The location accuracy is estimated
147 to be ± 5 mm.
148

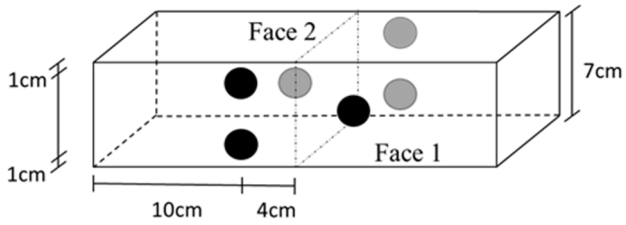

Figure 2: *3D AE transducers position (black sensors-face 1, grey sensors-face 2)*

3. Results and discussion

3.1. Effect of the percentage and the length of fibers on the fracture behavior

Three specimens have been tested for each mixture under three-point bending test to evaluate the repeatability. **Figure 3** presents the load versus the mid span deflection at the neutral axis for mixtures with three percentages and three lengths of flax fibers. The failure of earth concrete without fibers is brittle with an elastic phase followed by a high strength loss after reaching the peak indicating a fast propagation of the crack. For mixtures with fibers, an elastic phase has been also observed at the beginning. Then, the load drops after the peak due to the cracking of the matrix. This drop stops when the fibers, perpendicular to the crack path, are stretched and start to act in tension. This induces a resumption of stress and a nonlinear behavior is observed untill the second peak load. Note that, the load drop rate and strength recovery are highly dependent on the fibers distribution, orientation, length and quantity in earth concrete. The load recovery increases with the fiber's length and percentage. For SA03F50, SA06F24 and SA06F50, the strength drop is less important and specimens reached a second peak higher than the first one. This may be due to the efficiency of longer fibers to bridge the crack in comparison to the shorter ones that can be easily pulled out from earth concrete. Thus, long fibers allow the concrete to sustain higher loads and delay crack propagation in the specimen due to a higher anchor length. In addition, as the percentage of fibers increases, the probability of fibers presence at the crack level will increase which may also increase the fracture resistance due to a better stress redistribution and transfer between the matrix and the fibers.

In the softening part of specimens with flax fibers, the loss of stiffness is due to fibers being pull out from earth concrete and to micro cracking of concrete surrounding the initial crack and at the interface zone between the fibers and the matrix. This is responsible for the ductile failure and the high residual strength in the post peak region showing a good toughness and a post-crack resistance. In fact, the presence of flax fibers creates a bridge in the formed cracks and prevents any brittle rupture by redistributing the loads.

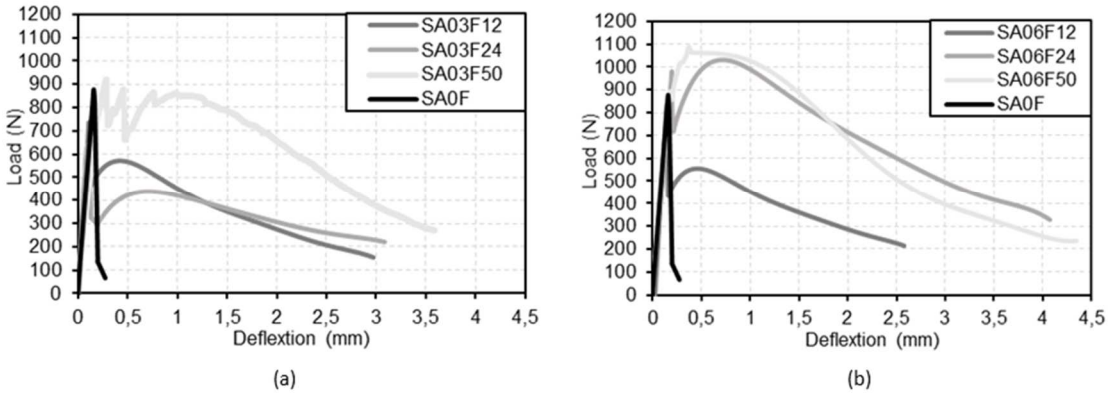

Figure 3: *Load - mid span deflection curves for SA0F (a) SA03F and (b) SA06F with different flax fibers lengths*

Figure 4 presents the flexural peak strength and the deflection at the highest peak for mixtures with different percentages and lengths of fibers. The net bending stress f_{net} at maximum loading is calculated using the following equation

$$f_{net} = \frac{6(F_{max}+\left(\frac{mg}{2}\right))}{4bh^2} \qquad \textbf{Equation 1}$$

where b is the thickness of the beam, h the height of the ligament, m is the weight of the specimen, l the span and F_{max} the maximum strength.

The flexural strength and the deflection at the peak load increase with mixtures containing a higher percentage of fibers with longer length. In fact, earth concrete becomes less rigid with an additional nonlinear phase before the second peak due to stress redistribution between the fibers and the matrix. Moreover, longer fibers provide sufficient length for an adequate bonding surface

with earth concrete matrix considering their position along the crack. A high variability has been observed for mixtures containing flax fibers with a length of 24 and 50 mm. This may be related to the random fiber distribution and orientation, to boundary effects, to the flexibility of flax fibers considering the shape and dimensions of earth concrete specimens, in addition to the possible segregation of fibers during mixing.

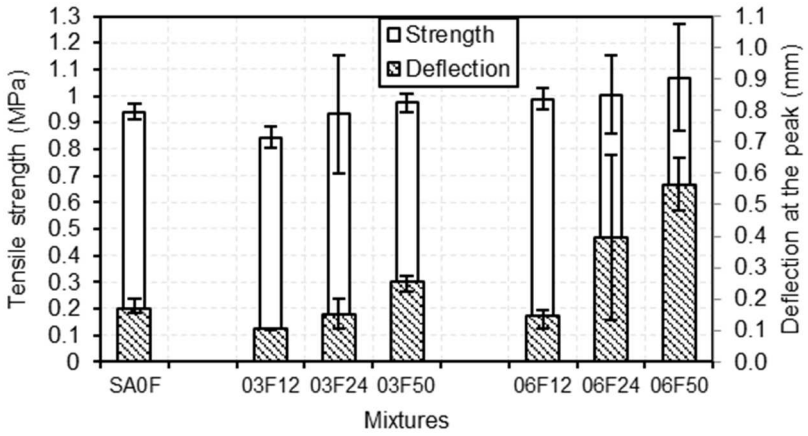

Figure 4: *Tensile strength and deflection at the peak for specimens with different lengths and percentages of flax fibers*

The elastic modulus and the fracture energy for the seven mixtures are also presented in **Figure 5**. The fracture energy (G_F [N.m^{-1}]) has been calculated according to Hillerborg [58] using the load-deflection curve. It is defined as the energy required to create a unit area of cracking surface and is equal to:

$$G_F = \frac{(w_0 + mg\delta_o)}{A_{lig}} \qquad \textbf{Equation 2}$$

where W_o [N.m] is the area under the load-deflection curve, m [kg]= m_1+ $2m_2$ with m_1 being the weight of the part of the specimen between the supports and m_2 the weight of the used loading arrangement, g [m/s^2] the acceleration due to gravity, δ_o the deformation at the final failure point and A_{lig} [m²] the area of the ligament.

Young's modulus (E) has been calculated using the load-deflection (Δ) curve according to the following formula:

$$E = \frac{\mathrm{F}_{\max} L^2}{4\Delta \mathrm{b} \mathrm{h}^3} \qquad \textbf{Equation 3}$$

The elastic modulus decreases slightly with the percentage of flax fibers; however, the fiber's length has no significant influence. The presence of fibers alters the pore distribution and total porosity of earth concrete as has been shown by mercury intrusion porosimetry, where the total porosity is equal to 35% for SA0F, 36% for the SA03F24 and 40% for the SA06F24 [14]. The fracture energy is equal to 65 $N.m^{-1}$ for SA0F and increases significantly with the percentage and length of flax fibers to reach a value of 770 $N.m^{-1}$ for SA06F50 (approximately 10 times higher). This indicates a higher energy absorption and a higher ductility due to different softening mechanisms induced by fibers.

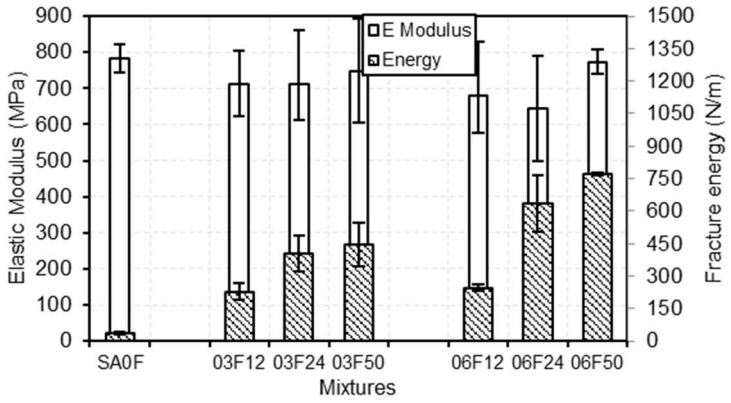

Figure 5: *Elastic modulus and fracture energy for specimens with different lengths and percentages of flax fibers*

To have a better understanding of the effect of fibers on the fracture process, the AE activity and the strain fields have been also analyzed for different loading levels.

3.2.AE activity analysis

Figure 6 presents the correlation between the load, amplitude and cumulative number of AE hits during the flexural tests for SA0F, SA03F24 and SA06F24. For SA0F, the AE activity is very low in the elastic phase. The detected signals may be due to the crushing of earth concrete at the contact with the press. The rate of the AE activity increases quickly at the peak with signals of high amplitudes due to the unstable propagation of the macro crack.

For mixtures with 0.3% and 0.6% of fibers, the evolution of the cumulative number of AE hits in correlation with the loading level can be sorted into four phases. During the elastic phase, the acoustic activity is low. Then, from the first peak and till the nonlinear phase of the second peak, the AE activity begins to increase slightly indicating the development of micro cracking. The generated signals have low amplitude and energy. The rate of the AE activity increases quickly after the peak indicating the propagation of a macro-crack. In the last phase, the rate of the AE activity decreases indicating a stable propagation of the crack. The signals generated during last phase present higher energy and amplitude. This may be due to additional damage mechanisms such as crack bridging, tearing and friction at the fiber/matrix interface due to fibers pullout [59]. Note that, the cumulative number of AE hits increases with the percentage of fibers.

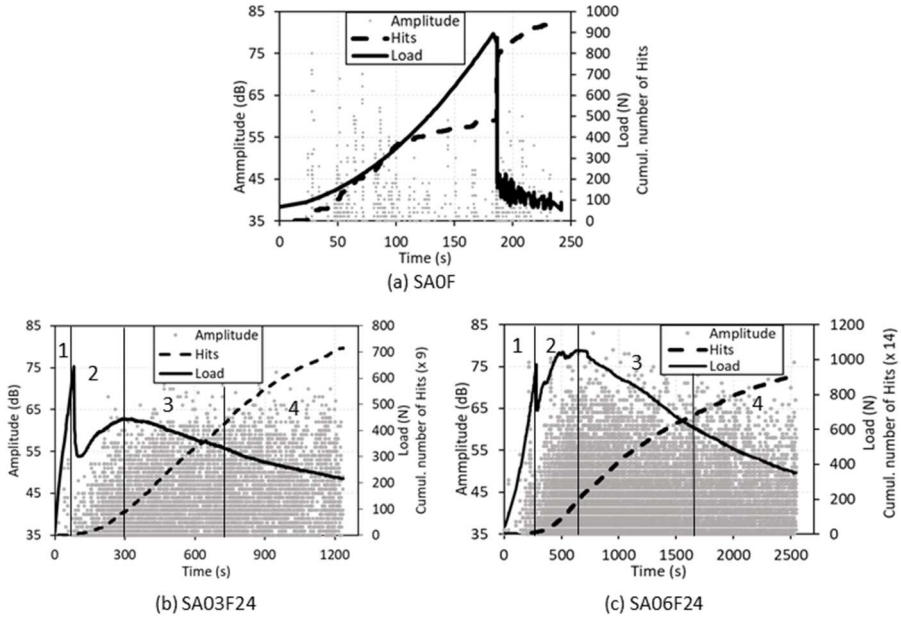

Figure 6: *Correlation between the load, the amplitude and the cumulative number of AE hits for SA0F (a), SA03F24 (b) and SA06F24 (c)*

The effect of the fiber's length on the AE activity has been also evaluated. **Figure 7** presents the correlation between the load and the cumulative number of AE hits for mixtures with 0.3% and 0.6% of different flax fiber lengths. The same phases distinguished before are observed. However, the total number of AE hits and the rate of AE activity increase with the fiber's length. This may be due to a larger fracture process zone (FPZ) as longer fibers may transfer load to a further distance which is also responsible for the higher fracture energy.

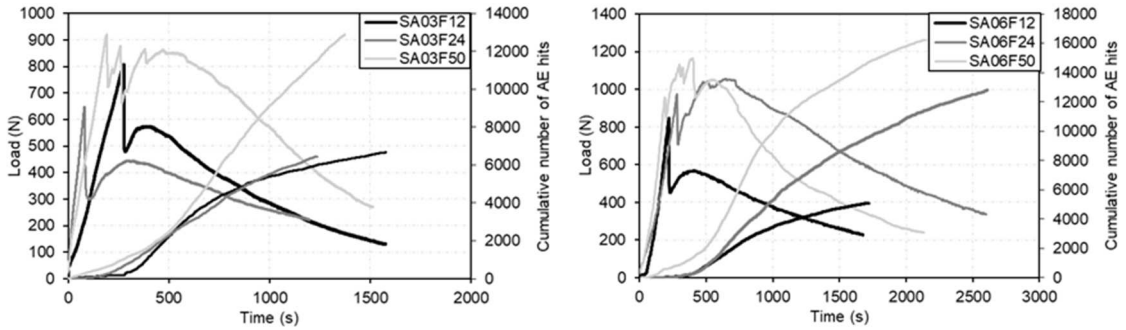

Figure 7: *Correlation between the load and the cumulative number of AE hits for (a) SA03F and (b) SA06F with different fiber lengths*

The total number of AE hits and the generated absolute AE energy (Abs. energy) for the seven mixtures increase with the fiber's percentage and length (**Figure 8)** which may be due to additional damage mechanisms, a larger FPZ and a greater energy absorption that limits crack propagation [60]. Note that, a higher variability has been also observed for specimens with fibers of higher length.

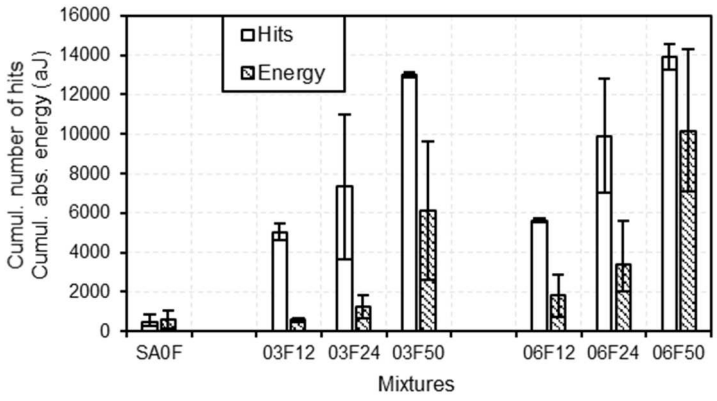

269

270 **Figure 8**: *Total number of AE hits and generated acoustic energy for specimens with different*
271 *lengths and percentages of flax fibers*

272

273 **Figure 9** presents the correlation between the absolute AE energy and the fracture energy. The
274 results show a good correlation between both types of energy in function of the percentage of
275 fibers. However, two different exponential relationships have been obtained for mixtures with
276 fibers of 24 and 50 mm. The least mean squares method has been used to minimize the error
277 between the proposed exponential function and the experimental measurements. The results show a
278 determination coefficient of about 0.95 and 0.92 for fibers of 24 and 50 mm respectively, indicating
279 a good correlation. Thus, the AE energy can provide valuable information about the fracture
280 properties of earth concrete.

281

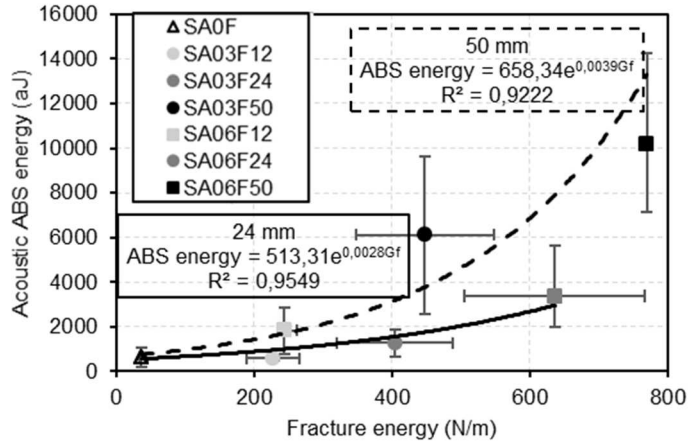

282

Figure 9: *Correlation between the AE energy and the fracture energy for specimens with different lengths and percentages of flax fibers*

In order to better evaluate the dimension of the FPZ, the AE localization maps and the strain fields have been also analyzed.

3.3. Correlation between AE and DIC results

A three-dimensional analysis is performed for the location of AE events representing the damage sources. The 3D localization algorithm is based on the difference between the arrival times at each transducer, the effective velocity, the geometry and the placement of sensors. For an AE event to be located in 3D, at least 4 waves must be detected.

Figure 10 presents the localization maps of AE events projected in 2D (m) and the 2D strain fields (mm/mm) along the X direction for SA0F, SA03F24 and SA06F24 at different loading levels. Four ranges of energy have been considered for the classification of AE events according to the rate of damage [61].

For SA0F, no AE events and no cracks have been detected before the peak. After the peak, the strain field shows a quick propagation of the crack till the rupture. However, only few AE events have been detected due to the brittle rupture of earth concrete. The detected AE events are due to the rupture of earth concrete matrix and present a good correlation with the position of the macro crack according to strain fields.

For mixtures with 0.3% and 0.6% of fibers, the crack initiated at the load drop. The DIC results show a quick propagation of a macro crack. However, the number of the detected AE events is very low due to the brittle rupture. The number of AE events started to increase slowly after the first peak in the nonlinear phase when the load was recovered by the presence of fibers and till the second peak. AE events are mainly located at the bottom of the beam where the stress is the most

significant. The crack length increased slowly in the post peak region due to load transfer between the matrix and flax fibers indicating good adhesion. The number of AE events increases with the loading level along the height of the beam indicating a continuous bond through the macro crack which is responsible for the slow crack propagation. This bond or fibers bridging prevented the brittle rupture of earth concrete.

The number of AE events increases with the percentage of flax fibers and reached 800 and 1000 events at 30% of the maximum strength in the post peak region for SA03F24 and SA06F24 respectively. This can be linked to the increase of the loaded contact points between flax fibers and earth concrete matrix.

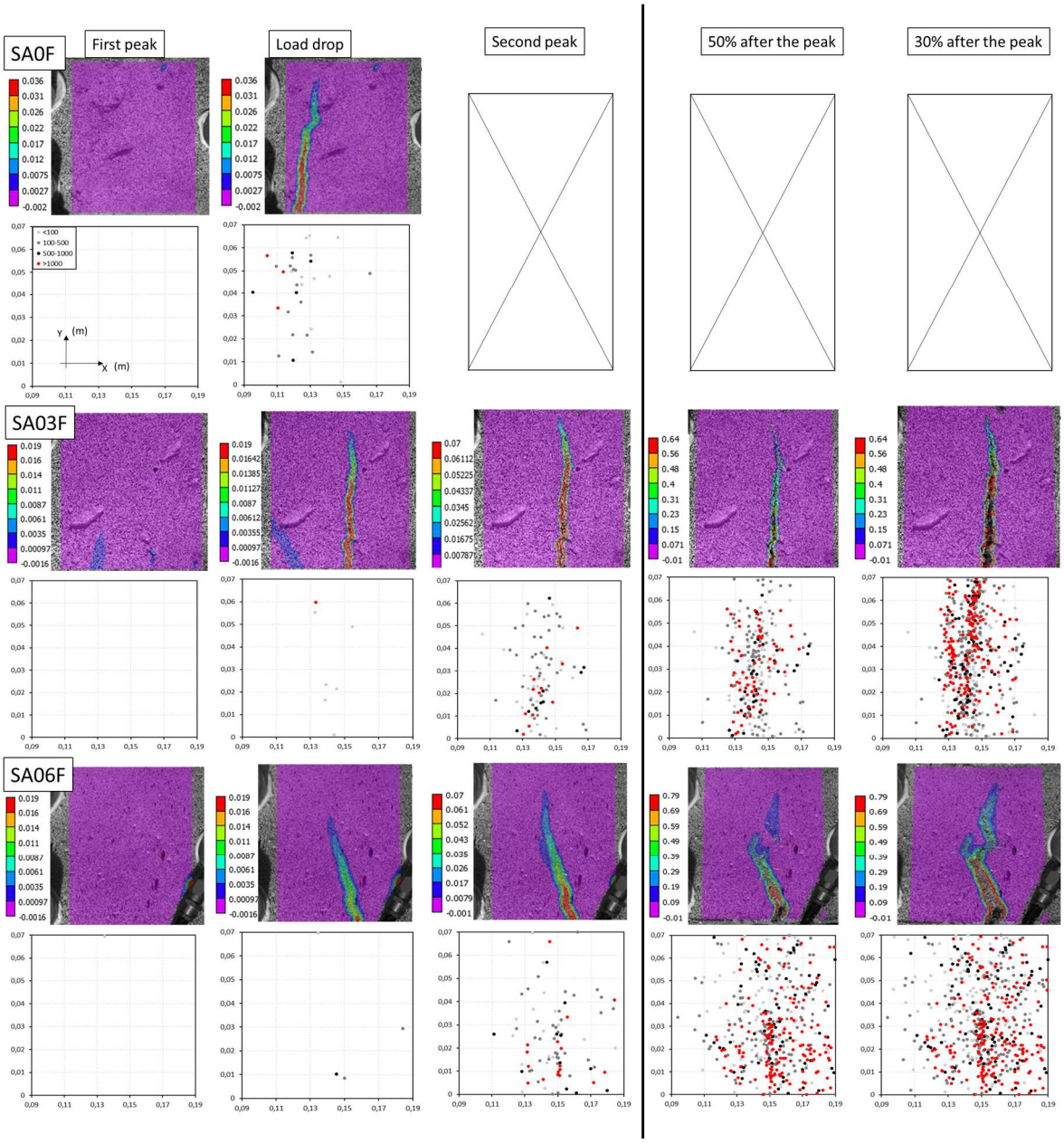

Figure 10: *AE events localization maps and strain fields for SA0F, SA03F24 and SA06F24*

The same analysis has been conducted to study the effect of fiber's length on the FPZ. **Figure 11** presents the 2D localization maps of AE events classified by their energy level and the strain fields for mixtures with 0.3% and 0.6% of fibers considering the three lengths at 30% of the maximum strength in the post peak region. For short fibers, AE events with high energy (the red points) are mainly located at the core of the FPZ. As the length of fibers increases, the width of AE events localization zone increases. In addition, AE events of higher energy are not only present

near the crack but also along the width of the FPZ due to friction between flax fibers and earth concrete. For SA06F50, the AE localization map showed an important concentration of energetic events in the middle of the specimen. This may be related to the segregation of flax fibers at this level as can be seen also with the strain field. Those energetic events can be associated to friction during the pull out of fibers as it has been shown in [59]. The stress concentration and the higher density of AE events at this level may be due to fiber segregation as can be seen at the fractured surfaces (figure 12).

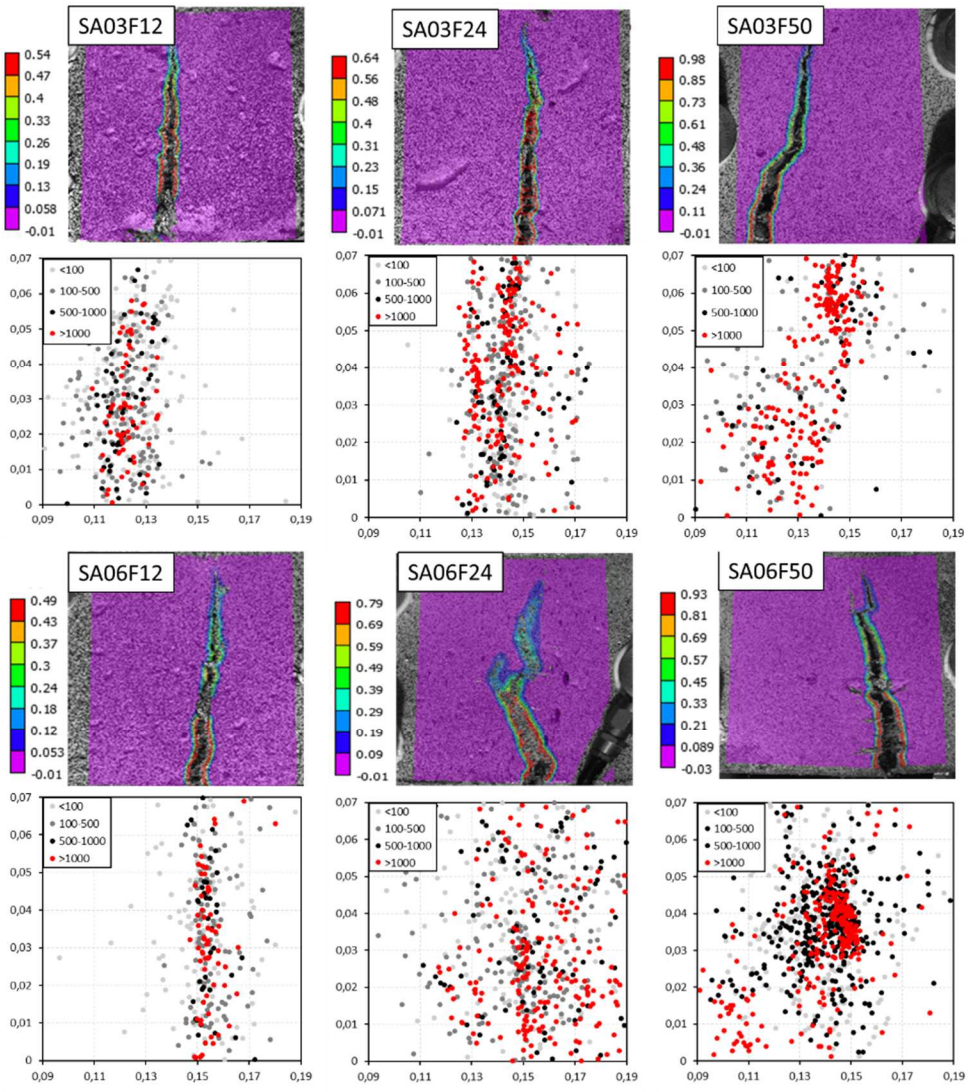

Figure 11: 2D *localization maps of AE events and strain fields for mixtures with 0.3% and 0.6% of flax fibers with different lengths*

Figure 12: *Fracture surfaces of SA06F50*

Figure 13 presents the recorded number of AE events according to their energy for mixtures with different percentages of flax fibers. For SA0F, the generated AE events presented low energy. For specimens with fibers, the number of energetic events increased with the loading level and the percentage of flax fibers indicating the advantage of using fibers for a better fracture resistance and energy absorption.

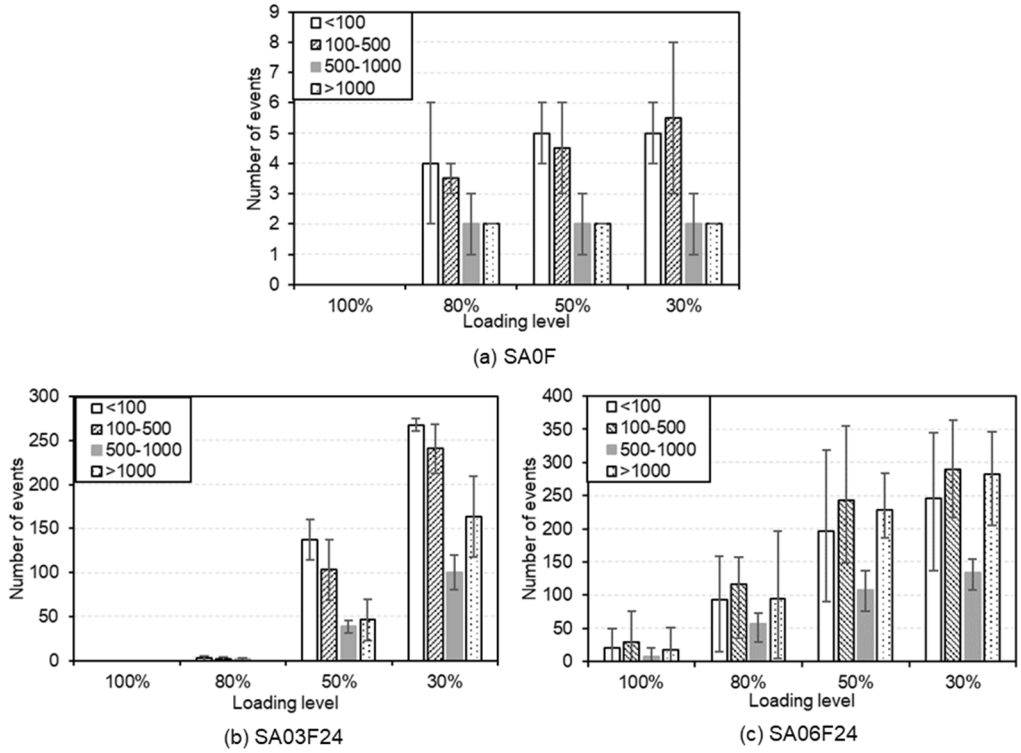

Figure 13: *Number of AE events according to their energies for (a) SA0F, (b) SA03F24 and (c) SA06F24 at different loading levels*

3.4. Effect of the fibers percentage and length on the fracture process zone

The evolution of the crack opening along the height of the specimens has been also analysed at different loading levels (**Figure 14**). It was obtained from the displacement across both sides of the crack [48]. For SA0F, the crack opening started to increase after the peak and varied almost linearly throughout the height of the specimen causing its brittle rupture. The crack developed quickly along the height and reached an opening equal to 0.175 mm in its largest point at the bottom of the specimen.

For SA03F24, the crack started to propagate at the load drop where it reached a length of 40 mm and increased slowly in the nonlinear phase to reach 52 mm at the second peak. After the second peak, the length of the crack continued to slightly increase to reach 64 mm along the height of the specimen with a high crack opening. For SA06F24, the crack also initiated at the load drop and reached a length of 20 mm. The length of the crack continued to increase reaching 33 mm at the second highest peak and 60 mm at 30% of the maximum strength in the post peak region. In the post peak region, the crack opening increased significantly due mainly to flax fibers pull out from earth concrete. The crack opening increased with the loading level and the percentage of fibers reached 3 and 4.3 mm at the bottom of the beam for SA03F24 and SA06F24 respectively at 30% of the maximum load in the post peak region. Thus, the crack length at the load drop decreased with the percentage of fibers while the deformation capacity and the crack propagation resistance increased.

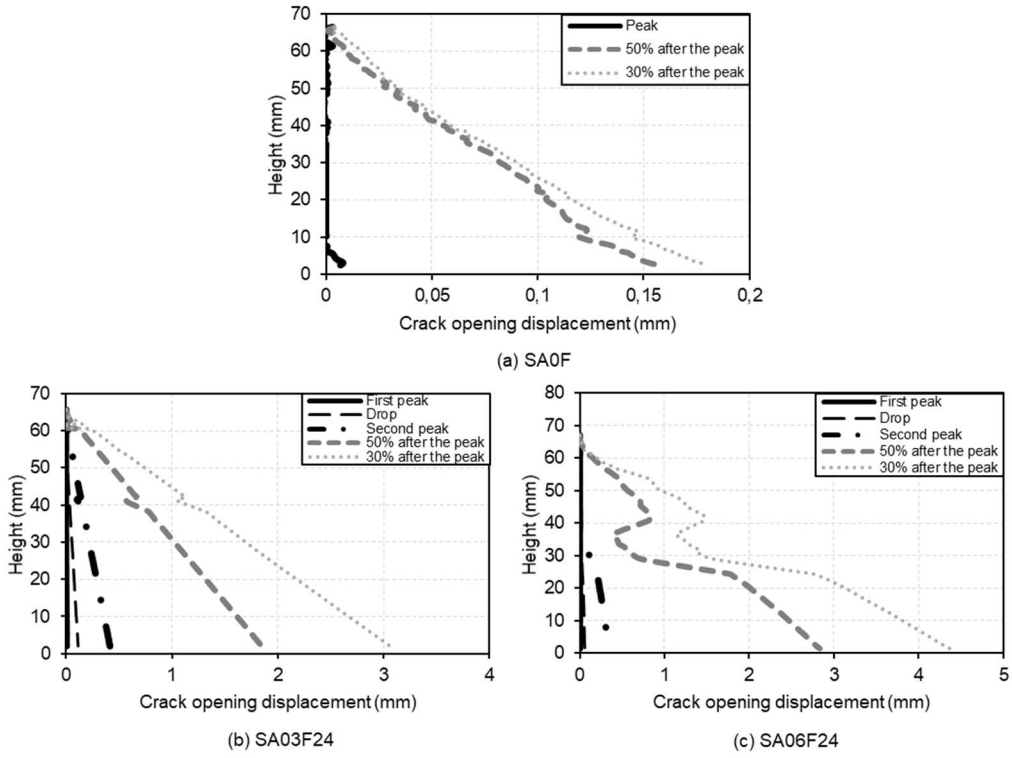

371

372 **Figure 14**: *Crack opening profile along the height of SA0F (a), SA03F24 (b) and SA06F24 (c) for*

373 *different loading level*

374

375

376 **Figure 15** presents the distribution of AE events along the X direction between 70 and 210 mm

377 resulting from AE events in Y and Z directions. The distribution of AE events shows a

378 concentration around the cracking zone and a gradual decrease on both sides of the crack. Based on

379 this distribution, the width of the FPZ is considered as the distance at the intersection between the

380 distribution of AE events and the line situated at 20% of the maximum value of AE events

381 distribution [24].

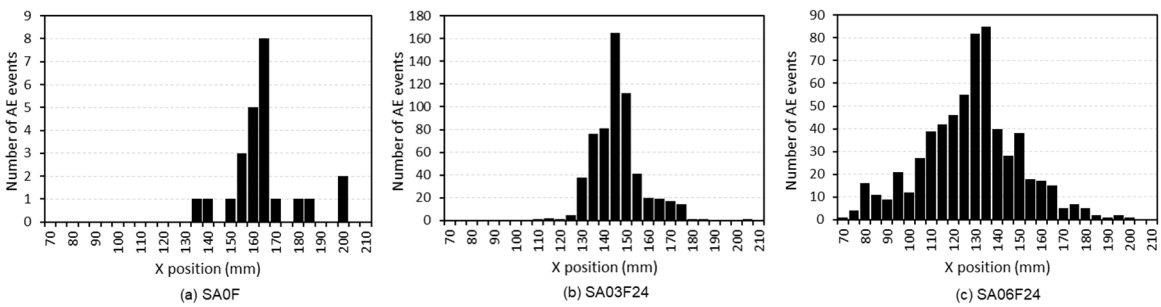

382

Figure 15: *Distribution of AE events in function of X for (a) SA0F, (b) SA03F24 and (c) SA06F24*

Figure 16 presents the width of the FPZ for specimens with different percentages and lengths of flax fibers. Due to the brittle failure of SA0F, the few AE events were distributed mainly where the failure occurred indicating a small FPZ width. The width of the FPZ increased with the length of fibers, however the effect of the percentage of fibers was found to be negligible. In fact, for long fibers and due to their higher bonding surface, more micro-cracks appeared during the deboning of fibers.

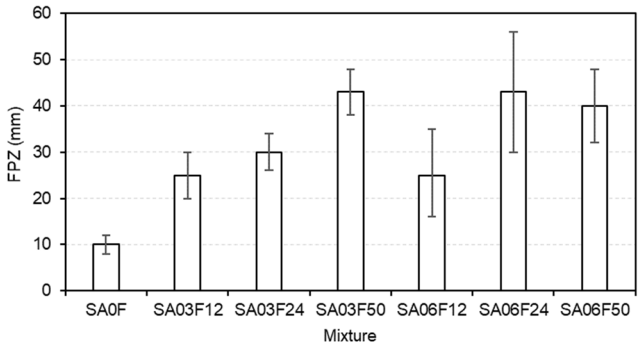

Figure 16: *Fracture process zone width for mixtures with different percentages and lengths of flax fibers*

3.5.Damage source identification by AE analysis

The shape of AE signals can be used to define the crack mode [62]. RA-AF association diagram has been widely used to determine the shear and tensile failure modes [28,63,64]. The RA parameter expressed in µs/V is defined as the ration between the rise time and amplitude. The AF in kHz is defined as the number of counts divided by the duration of the signal. The RA value of shear cracks failure is higher than the one obtained during tensile crack failure while the average frequency is lower [38,65,66].

Figure 17 presents the evolution of RA and AF during the loading process for SA0F, SA03F24 and SA06F24. Each point of the curve represents the average parameter of 100 signals.

For SA0F, only the elastic phase is considered as specimens failed suddenly after reaching the peak. The results show a fluctuation of AF and RA due to the crushing of concrete at the press contact generating shear cracks. For specimens with fibers, AF begins to increase as the force drops while RA increases, indicating mainly a tensile mode failure attributed to matrix cracking and the rupture of the chemical adhesion between the fibers and earth concrete. Then, a sharp decrease of AF is observed in the nonlinear phase (while RA increases) indicating the slip of flax fibers and remains low in the post peak region indicating shear cracks due to friction during fibers pull out.

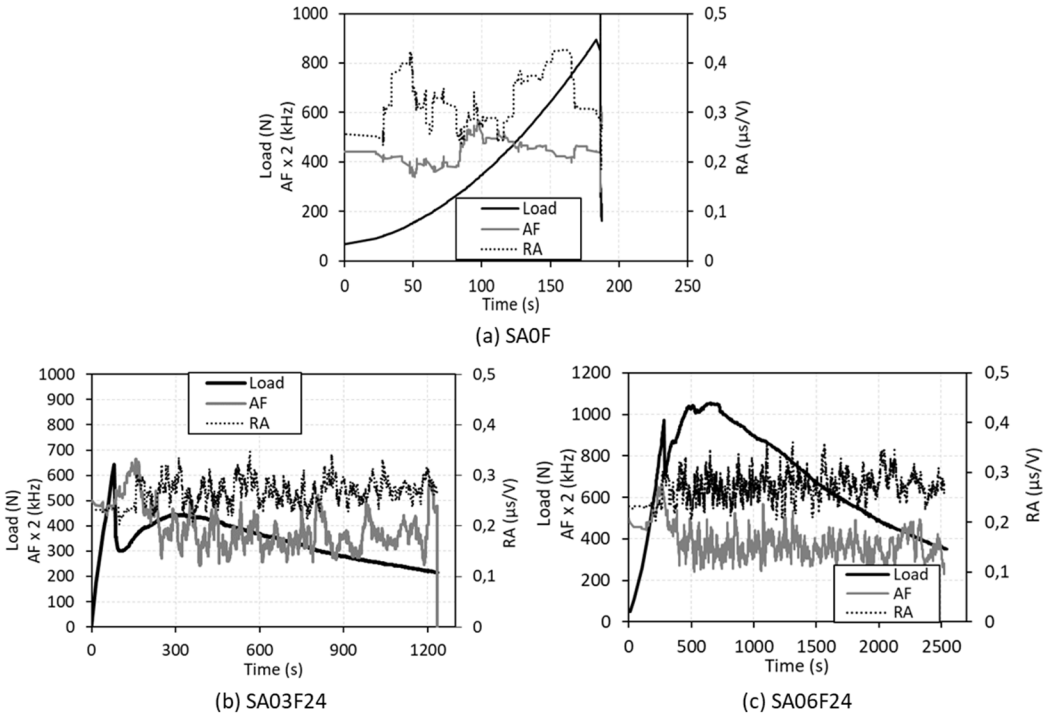

Figure 17: *Evolution of AF and RA in correlation with the load for (a) SA0F, (b) SA03F24 and (c) SA06F24.*

Figure 18 presents the variation of RA-AF for SA0F, SA03F24 and SA06F24. The variation of RA and AF are studied according to the different phases described before: phase 1: till the peak load; phase 2: the drop of the load and till the second peak; phase 3: the post peak region with high rate of AE activity and phase 4: the softening region when the rate of the AE activity starts to decrease. The variation of AF / RA can be divided in two zones that separate the signals

generated by shear and tensile failure. The dotted line represents the boundary separating those zones. This line depends on the properties of the tested material, the applied load, the dimension and the geometry of specimens. For specimens with fibers, the number of AE hits with high RA value and low frequency increased mainly in phases 3 and 4 indicating that damage is mainly due to shear rupture as indicated in **figure 17**. In fact, stresses are mainly transferred in these phases through flax fibers and cracking may be due to the friction at the interface between earth concrete and flax fibers [31,34]. Tensile cracks have been also generated during those phases which may be due to radial cracking in earth concrete generated during fibers pull out in addition to fibers orientation. The same phases have been observed with the variation of the fiber length. However, an increase of the number of signals with higher RA and lower AF has been observed as the fiber length increases indicating a larger number of shear cracks.

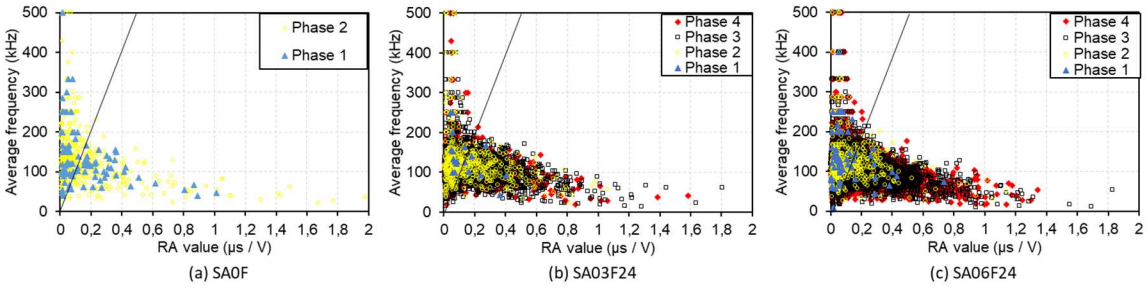

Figure 18: *Evolution of AE in function of RA for (a) SA0F, (b) SA03F24 and (c) SA06F24.*

4. Conclusions and perspectives

An experimental program has been conducted in this paper in order to study the effect of the percentage and length of flax fibers on the fracture behavior of earth concrete. Flexural tests have been monitored in parallel with the DIC and the AE techniques. Based on the obtained results, the following conclusions can be listed:

- Earth concrete presents a brittle failure and a low deformation capacity. The addition of flax fibers allows to enhance the ductility of earth concrete due to load redistribution and bridging effect of fibers.

445 • The fracture properties as the tensile strength, the deflection at the peak and the fracture
446 energy increased with the percentage and the length of flax fibers.
447 • The cumulative number of AE hits increased with the percentage and the length of flax
448 fibers due to additional damage mechanisms and a higher FPZ width.
449 • The DIC validated the results obtained with the AE technique concerning the crack
450 location and allowed to measure the crack opening that increased with the percentage of fibers.
451 • The AF-RA curves have been used to identify the shear and tensile failure modes during
452 rupture. Shear cracks increased with fibers addition due to friction during fibers pull out.
453 An additional study will be realized in the future in order to better classify the various damage
454 mechanisms based on a multivariable statistical analysis and evaluate the durability of the
455 reinforced earth concrete.
456

457 **References**

458 [1] F. Asdrubali, F.D. Alessandro, S. Schiavoni, Sustainable Materials and Technologies A
459 review of unconventional sustainable building insulation materials, SUSMAT. 4 (2020) 1–
460 17. https://doi.org/10.1016/j.susmat.2015.05.002.
461 [2] H. Dahlbo, J. Bachér, K. Lähtinen, T. Jouttijärvi, P. Suoheimo, T. Mattila, S. Sironen, T.
462 Myllymaa, K. Saramäki, Construction and demolition waste management - A holistic
463 evaluation of environmental performance, J. Clean. Prod. 107 (2015) 333–341.
464 https://doi.org/10.1016/j.jclepro.2015.02.073.
465 [3] L. Pérez-Lombard, J. Ortiz, C. Pout, A review on buildings energy consumption
466 information, Energy Build. 40 (2008) 394–398.
467 https://doi.org/10.1016/j.enbuild.2007.03.007.
468 [4] G. Ramakrishna, T. Sundararajan, Impact strength of a few natural fibre reinforced cement
469 mortar slabs : a comparative study, 27 (2005) 547–553.
470 https://doi.org/10.1016/j.cemconcomp.2004.09.006.
471 [5] A. Agarwal, B. Nanda, D. Maity, Experimental investigation on chemically treated bamboo

reinforced concrete beams and columns, Constr. Build. Mater. 71 (2014) 610–617. https://doi.org/10.1016/j.conbuildmat.2014.09.011.

[6] J. Claramunt, R. Dias, T. Filho, Cellulosic fiber reinforced cement-based composites : A review of recent, 79 (2015) 115–128. https://doi.org/10.1016/j.conbuildmat.2015.01.035.

[7] J. Page, F. Khadraoui, M. Boutouil, M. Gomina, Multi-physical properties of a structural concrete incorporating short flax fibers, Constr. Build. Mater. 140 (2017) 344–353. https://doi.org/10.1016/j.conbuildmat.2017.02.124.

[8] C. Llatas, A model for quantifying construction waste in projects according to the European waste list, Waste Manag. 31 (2011) 1261–1276. https://doi.org/10.1016/j.wasman.2011.01.023.

[9] H. Van Damme, H. Houben, Earth concrete. Stabilization revisited, Cem. Concr. Res. 114 (2016) 90–102. https://doi.org/10.1016/j.cemconres.2017.02.035.

[10] E.O. Momoh, A.I. Osofero, Behaviour of oil palm broom fibres (OPBF) reinforced concrete, Constr. Build. Mater. 221 (2019) 745–761. https://doi.org/10.1016/j.conbuildmat.2019.06.118.

[11] N. Benmansour, B. Agoudjil, A. Gherabli, A. Kareche, Thermal and mechanical performance of natural mortar reinforced with date palm fibers for use as insulating materials in building, Energy Build. 81 (2014) 98–104. https://doi.org/10.1016/j.enbuild.2014.05.032.

[12] S.K. Al-Oraimi, A.C. Seibi, Mechanical characterisation and impact behaviour of concrete reinforced with natural fibres, Compos. Struct. 32 (1995) 165–171.

[13] C.A.S. Hill, H.P.S.A. Khalil, M.D. Hale, A study of the potential of acetylation to improve the properties of plant fibres, Ind. Crops Prod. 8 (1998) 53–63. https://doi.org/10.1016/S0926-6690(97)10012-7.

[14] N. Kouta, J. Saliba, N. Saiyouri, Effect of flax fibers on early age shrinkage and cracking of earth concrete, Constr. Build. Mater. 254 (2020) 119315. https://doi.org/10.1016/j.conbuildmat.2020.119315.

499 [15] P. Sta, J.G.M. Van Mier, Manufacturing , fibre anisotropy and fracture of hybrid fibre
500 concrete, 74 (2007) 223–242. https://doi.org/10.1016/j.engfracmech.2006.01.028.
501 [16] A. Pompo, P.R. Stupak, L. Nicolais, B. Marchese, Analysis of Steel Fibre Pull-Out from a
502 Cement Matrix Using Video Photography, 9465 (1996) 3–8.
503 [17] S.R. Pemberton, E.K. Oberg, J. Dean, D. Tsarouchas, A.E. Markaki, L. Marston, T.W.
504 Clyne, The fracture energy of metal fibre reinforced ceramic composites (MFCs), Compos.
505 Sci. Technol. 71 (2011) 266–275. https://doi.org/10.1016/j.compscitech.2010.10.011.
506 [18] I. Pavasars, J. Hagberg, H. Borén, B. Allard, Alkaline Degradation of Cellulose : Mechanisms and Kinetics, J. Polym. Environ. 11 (2003).
508 [19] R. Dias, T. Filho, F.D.A. Silva, E.M.R. Fairbairn, J. De Almeida, M. Filho, Durability of
509 compression molded sisal fiber reinforced mortar laminates, Constr. Build. Mater. 23 (2009)
510 2409–2420. https://doi.org/10.1016/j.conbuildmat.2008.10.012.
511 [20] J. Wei, C. Meyer, Degradation mechanisms of natural fi ber in the matrix of cement
512 composites, Cem. Concr. Res. 73 (2015) 1–16.
513 https://doi.org/10.1016/j.cemconres.2015.02.019.
514 [21] M. Bouhicha, F. Aouissi, S. Kenai, Performance of composite soil reinforced with barley
515 straw, Cem. Concr. Compos. 27 (2005) 617–621.
516 https://doi.org/10.1016/j.cemconcomp.2004.09.013.
517 [22] K. Ghavami, R.D. Toledo Filho, N.P. Barbosa, Behaviour of composite soil reinforced with
518 natural fibres, Cem. Concr. Compos. 21 (1999) 39–48. https://doi.org/10.1016/S0958-
519 9465(98)00033-X.
520 [23] A.E.M.K. Mohamed, Improvement of swelling clay properties using hay fibers, Constr.
521 Build. Mater. 38 (2013) 242–247. https://doi.org/10.1016/j.conbuildmat.2012.08.031.
522 [24] A. Boniface, J. Saliba, Z.M. Sbartaï, N. Ranaivomanana, J.P. Balayssac, Evaluation of the
523 acoustic emission 3D localisation accuracy for the mechanical damage monitoring in
524 concrete, Eng. Fract. Mech. 223 (2020) 106742.
525 https://doi.org/10.1016/j.engfracmech.2019.106742.

526 [25] Q. Dai, K. Ng, J. Zhou, E.L. Kreiger, T.M. Ahlborn, Damage investigation of single-edge
527 notched beam tests with normal strength concrete and ultra high performance concrete
528 specimens using acoustic emission techniques, Constr. Build. Mater. 31 (2012) 231–242.
529 https://doi.org/10.1016/j.conbuildmat.2011.12.080.
530 [26] K. Ohno, K. Uji, A. Ueno, M. Ohtsu, Fracture process zone in notched concrete beam under
531 three-point bending by acoustic emission, Constr. Build. Mater. 67 (2014) 139–145.
532 https://doi.org/10.1016/j.conbuildmat.2014.05.012.
533 [27] S. De Sutter, S. Verbruggen, T. Tysmans, D.G. Aggelis, Fracture monitoring of lightweight
534 composite-concrete beams, Compos. Struct. 167 (2017) 11–19.
535 https://doi.org/10.1016/j.compstruct.2017.01.024.
536 [28] K. Ohno, M. Ohtsu, Crack classification in concrete based on acoustic emission, Constr.
537 Build. Mater. 24 (2010) 2339–2346. https://doi.org/10.1016/j.conbuildmat.2010.05.004.
538 [29] S. Li, X. Fan, X. Chen, S. Liu, Y. Guo, Development of fracture process zone in full-graded
539 dam concrete under three-point bending by DIC and acoustic emission, Eng. Fract. Mech.
540 230 (2020) 106972. https://doi.org/10.1016/j.engfracmech.2020.106972.
541 [30] D.G. Aggelis, S. De Sutter, S. Verbruggen, E. Tsangouri, T. Tysmans, Acoustic emission
542 characterization of damage sources of lightweight hybrid concrete beams, Eng. Fract. Mech.
543 210 (2019) 181–188. https://doi.org/10.1016/j.engfracmech.2018.04.019.
544 [31] D. Soulioti, N.M. Barkoula, A. Paipetis, T.E. Matikas, T. Shiotani, D.G. Aggelis, Acoustic
545 emission behavior of steel fibre reinforced concrete under bending, Constr. Build. Mater. 23
546 (2009) 3532–3536. https://doi.org/10.1016/j.conbuildmat.2009.06.042.
547 [32] J. Saliba, A. Loukili, F. Grondin, J.P. Regoin, Identification of damage mechanisms in
548 concrete under high level creep by the acoustic emission technique, Mater. Struct. Constr.
549 47 (2014) 1041–1053. https://doi.org/10.1617/s11527-013-0113-6.
550 [33] J. Saliba, M. Matallah, A. Loukili, J.P. Regoin, D. Grégoire, L. Verdon, G. Pijaudier-Cabot,
551 Experimental and numerical analysis of crack evolution in concrete through acoustic
552 emission technique and mesoscale modelling, Eng. Fract. Mech. 167 (2016) 123–137.

553 https://doi.org/10.1016/j.engfracmech.2016.03.044.
554 [34] T. Shiotani, Evaluation of long-term stability for rock slope by means of acoustic emission
555 technique, 39 (2006) 217–228. https://doi.org/10.1016/j.ndteint.2005.07.005.
556 [35] D.G. Aggelis, A.C. Mpalaskas, T.E. Matikas, Investigation of different fracture modes in
557 cement-based materials by acoustic emission, Cem. Concr. Res. 48 (2013) 1–8.
558 https://doi.org/10.1016/j.cemconres.2013.02.002.
559 [36] M.A. Rasheed, S.S. Prakash, G. Raju, Y. Kawasaki, Fracture studies on synthetic fiber
560 reinforced cellular concrete using acoustic emission technique, Constr. Build. Mater. 169
561 (2018) 100–112. https://doi.org/10.1016/j.conbuildmat.2018.02.157.
562 [37] D.G. Aggelis, D. V Soulioti, N.M. Barkoula, A.S. Paipetis, T.E. Matikas, Influence of fiber
563 chemical coating on the acoustic emission behavior of steel fiber reinforced concrete, Cem.
564 Concr. Compos. 34 (2012) 62–67. https://doi.org/10.1016/j.cemconcomp.2011.07.003.
565 [38] A. Bhosale, M.A. Rasheed, S.S. Prakash, G. Raju, A study on the efficiency of steel vs .
566 synthetic vs . hybrid fibers on fracture behavior of concrete in flexure using acoustic
567 emission, Constr. Build. Mater. 199 (2019) 256–268.
568 https://doi.org/10.1016/j.conbuildmat.2018.12.011.
569 [39] H. Xargay, P. Folino, N. Nuñez, M. Gómez, A. Caggiano, Acoustic Emission behavior of
570 thermally damaged Self-Compacting High Strength Fiber Reinforced Concrete, 187 (2018)
571 519–530. https://doi.org/10.1016/j.conbuildmat.2018.07.156.
572 [40] R. Kravchuk, E.N. Landis, Acoustic emission-based classification of energy dissipation
573 mechanisms during fracture of fiber-reinforced ultra-high-performance concrete, Constr.
574 Build. Mater. 176 (2018) 531–538. https://doi.org/10.1016/j.conbuildmat.2018.05.039.
575 [41] B. Li, L. Xu, Y. Shi, Y. Chi, Q. Liu, C. Li, Effects of fiber type , volume fraction and aspect
576 ratio on the flexural and acoustic emission behaviors of steel fiber reinforced concrete,
577 Constr. Build. Mater. 181 (2018) 474–486.
578 https://doi.org/10.1016/j.conbuildmat.2018.06.065.
579 [42] D.G. Aggelis, D. V Soulioti, E.A. Gatselou, N. Barkoula, T.E. Matikas, Monitoring of the

mechanical behavior of concrete with chemically treated steel fibers by acoustic emission, Constr. Build. Mater. 48 (2013) 1255–1260. https://doi.org/10.1016/j.conbuildmat.2012.06.066.

[43] T.M. Fayyad, J.M. Lees, Experimental investigation of crack propagation and crack branching in lightly reinforced concrete beams using digital image correlation, Eng. Fract. Mech. 182 (2017) 487–505. https://doi.org/10.1016/j.engfracmech.2017.04.051.

[44] M.D.C. Ferreira, W.S. Venturini, F. Hild, On the analysis of notched concrete beams: From measurement with digital image correlation to identification with boundary element method of a cohesive model, Eng. Fract. Mech. 78 (2011) 71–84. https://doi.org/10.1016/j.engfracmech.2010.10.008.

[45] Y. Zhao, L. Wang, Z. Lei, X. Han, J. Shi, Study on bending damage and failure of basalt fiber reinforced concrete under freeze-thaw cycles, Constr. Build. Mater. 163 (2018) 460–470. https://doi.org/10.1016/j.conbuildmat.2017.12.096.

[46] Y. Zhao, L. Wang, Z. Lei, X. Han, Y. Xing, Experimental study on dynamic mechanical properties of the basalt fiber reinforced concrete after the freeze-thaw based on the digital image correlation method, Constr. Build. Mater. 147 (2017) 194–202. https://doi.org/10.1016/j.conbuildmat.2017.02.133.

[47] W. Dong, Z. Wu, X. Zhou, N. Wang, G. Kastiukas, An experimental study on crack propagation at rock-concrete interface using digital image correlation technique, Eng. Fract. Mech. 171 (2017) 50–63. https://doi.org/10.1016/j.engfracmech.2016.12.003.

[48] S. Yasir, J. Saliba, A. Loukili, Fracture examination in concrete through combined digital image correlation and acoustic emission techniques, Constr. Build. Mater. 69 (2014) 232–242. https://doi.org/10.1016/j.conbuildmat.2014.07.044.

[49] Z. Wu, H. Rong, J. Zheng, F. Xu, W. Dong, An experimental investigation on the FPZ properties in concrete using digital image correlation technique, Eng. Fract. Mech. 78 (2011) 2978–2990. https://doi.org/10.1016/j.engfracmech.2011.08.016.

[50] B. Liu, J. Guo, X. Wen, J. Zhou, Z. Deng, Study on flexural behavior of carbon fibers

607 reinforced coral concrete using digital image correlation, Constr. Build. Mater. 242 (2020)
608 117968. https://doi.org/10.1016/j.conbuildmat.2019.117968.
609 [51] F.G. Bell, Lime stabilization of clay minerals and soils, Eng. Geol. 42 (1996) 223–237.
610 https://doi.org/10.1016/0013-7952(96)00028-2.
611 [52] S.A. Khattab, M. Al-Mukhtar, J.M. Fleureau, Long-term stability characteristics of a lime-
612 treated plastic soil, J. Mater. Civ. Eng. 19 (2007) 358–366.
613 [53] C.A. Anagnostopoulos, Strength properties of an epoxy resin and cement-stabilized silty
614 clay soil, Appl. Clay Sci. 114 (2015) 517–529. https://doi.org/10.1016/j.clay.2015.07.007.
615 [54] D.C. Ngo, J. Saliba, N. Saiyouri, Z.M. Sbartaï, Design of a soil concrete as a new building
616 material – Effect of clay and hemp proportions, J. Build. Eng. 32 (2020) 101553.
617 https://doi.org/10.1016/j.jobe.2020.101553.
618 [55] J. Page, F. Khadraoui, M. Gomina, M. Boutouil, Influence of different surface treatments on
619 the water absorption capacity of flax fibres : Rheology of fresh reinforced-mortars and
620 mechanical properties in the hardened state, Constr. Build. Mater. 199 (2019) 424–434.
621 https://doi.org/10.1016/j.conbuildmat.2018.12.042.
622 [56] L. Yan, N. Chouw, K. Jayaraman, Flax fibre and its composites - A review, Compos. Part B
623 Eng. 56 (2014) 296–317. https://doi.org/10.1016/j.compositesb.2013.08.014.
624 [57] U. Huner, Effect of Water Absorption on the Mechanical Properties \of Flax Fiber
625 Reinforced Epoxy Composites, Adv. Sci. Technol. Res. J. 9 (2015) 1–6.
626 https://doi.org/10.12913/22998624/2357.
627 [58] A. Hillerborg, The theoretical basis of a method to determine the fracture energy GF of
628 concrete, Mater. Struct. 18 (1985) 291–296. https://doi.org/10.1007/BF02472919.
629 [59] J. Saliba, D. Mezhoud, Monitoring of steel-concrete bond with the acoustic emission
630 technique, Theor. Appl. Fract. Mech. 100 (2019) 416–425.
631 https://doi.org/10.1016/j.tafmec.2019.01.034.
632 [60] F. Aymerich, L. Fenu, P. Meloni, Effect of reinforcing wool fibres on fracture and energy
633 absorption properties of an earthen material, Constr. Build. Mater. 27 (2012) 66–72.

https://doi.org/10.1016/j.conbuildmat.2011.08.008.

[61] S. Muralidhara, B.K.R. Prasad, H. Eskandari, B.L. Karihaloo, Fracture process zone size and true fracture energy of concrete using acoustic emission, Constr. Build. Mater. 24 (2010) 479–486. https://doi.org/10.1016/j.conbuildmat.2009.10.014.

[62] D.G. Aggelis, Classification of cracking mode in concrete by acoustic emission parameters, Mech. Res. Commun. 38 (2011) 153–157. https://doi.org/10.1016/j.mechrescom.2011.03.007.

[63] X. Zhang, W. Shan, Z. Zhang, B. Li, AE monitoring of reinforced concrete squat wall subjected to cyclic loading with information entropy-based analysis, Eng. Struct. 165 (2018) 359–367. https://doi.org/10.1016/j.engstruct.2018.03.059.

[64] J. Xu, S. Shu, Q. Han, C. Liu, Experimental research on bond behavior of reinforced recycled aggregate concrete based on the acoustic emission technique, Constr. Build. Mater. 191 (2018) 1230–1241. https://doi.org/10.1016/j.conbuildmat.2018.10.054.

[65] C. Chen, X. Fan, X. Chen, Experimental investigation of concrete fracture behavior with different loading rates based on acoustic emission, Constr. Build. Mater. 237 (2020) 117472. https://doi.org/10.1016/j.conbuildmat.2019.117472.

[66] N. Ranjbar, A. Behnia, H. Kian, U.J. Alengaram, M. Zamin, Fracture evaluation of multi-layered precast reinforced geopolymer- concrete composite beams by incorporating acoustic emission into mechanical analysis, 127 (2016) 274–283. https://doi.org/10.1016/j.conbuildmat.2016.09.144.

[67] T.P. Philippidis, V.N. Nikolaidis, A.A. Anastassopoulos, Damage characterization of carbon / carbon laminates using neural network techniques on AE signals, 31 (1998) 329–340.